J Shoulder Elbow Surg (2020) 29, 1460–1469

ELSEVIER

Journal of Shoulder and Elbow Surgery

www.elsevier.com/locate/ymse

Type E2 glenoid bone loss orientation and management with augmented implants

Sejla Abdic, BSc, MD[a,b], Nikolas K. Knowles, PhD[b,c], Gilles Walch, MD[d], James A. Johnson, PhD, PEng[b,e], George S. Athwal, MD, FRCSC[b,e,f,*]

[a]*Department of Orthopaedics and Traumatology, Paracelsus Medical University, Salzburg, Austria*
[b]*Roth|McFarlane Hand and Upper Limb Centre, St Joseph's Hospital, London, ON, Canada*
[c]*School of Biomedical Engineering, Western University, London, ON, Canada*
[d]*Hôpital Privé Jean-Mermoz–GDS Ramsay, Lyon, France*
[e]*Department of Surgery, Western University, London, ON, Canada*
[f]*Division of Orthopaedic Surgery, London Health Sciences Center, London, ON, Canada*

Background: The purpose of this study was 2-fold: (1) to quantify type E2 bone loss orientation and its association with rotator cuff fatty infiltration and (2) to examine reverse baseplate designs used to manage type E2 glenoids.

Methods: Computed tomography scans of 40 patients with type E2 glenoids were examined for pathoanatomic features and erosion orientation. The rotator cuff fatty infiltration grade was compared with the erosion orientation angle. To compare reconstructive options in light of the pathoanatomic findings, virtual implantation of 4 glenoid baseplate designs (standard, half wedge, full wedge, and patient-matched) was conducted to determine the volume of bone removal for seating and impingement-free range of motion.

Results: The mean type E2 erosion orientation angle was 47° ± 17° from the 0° superoinferior glenoid axis, resulting in the average erosion being located in the posterosuperior quadrant directed toward the 10:30 clock-face position. The type E2 neoglenoid, on average, involved 67% of the total glenoid surface (total surface area, 946 ± 209 mm^2; neoglenoid surface area, 636 ± 247 mm^2). The patient-matched baseplate design resulted in significantly ($P \leq .01$) less bone removal (200 ± 297 mm^3) for implantation, followed by the full-wedge design (1228 ± 753 mm^3), half-wedge design (1763 ± 969 mm^3), and standard (non-augmented) design (4009 ± 1210 mm^3). We noted a marked difference in erosion orientation toward a more superior direction as the subscapularis fatty infiltration grade increased from grade 3 to grade 4 ($P < .001$).

Conclusion: The average type E2 erosion orientation was directed toward the 10:30 clock-face position in the posterosuperior glenoid quadrant. This orientation resulted in the patient-matched glenoid augmentation requiring the least amount of bone removal for seating, followed by the full-wedge, half-wedge, and standard designs. Implant selection also substantially affected computationally derived range of motion in external rotation, flexion, extension, and adduction.

No institutional review board approval was required for this computer modeling study.

*Reprint requests: George S. Athwal, MD, FRCSC, St Joseph's Health Care, Western University, 268 Grosvenor St, London, ON N6A 4L6, Canada.

E-mail address: gathwal@uwo.ca (G.S. Athwal).

https://doi.org/10.1016/j.jse.2019.11.009

Level of evidence: Basic Science Study; Anatomy Imaging and Computer Modeling

Keywords: Glenoid; E2; cuff tear arthropathy; reverse shoulder arthroplasty; augmented implants; BIO-RSA; bone loss; implant design

Glenoid pathoanatomic changes can occur after long-term muscular imbalance associated with chronic rotator cuff insufficiency. Some authors have described the incidence of pathologic bone remodeling in the context of cuff tear arthropathy nearing 40%,[6,12,19] but knowledge on the true incidence and severity of glenoid pathoanatomic changes is limited. Frankle et al[6] reported that among all acquired glenoid bone loss scenarios undergoing reverse shoulder arthroplasty, superior glenoid erosion (termed "type E2" by the Favard classification[21]) was the second most common erosion pattern, after type B2. Type E2 erosion is caused by chronic superior migration of the humeral head owing to a lack of constraint normally provided by the compressive forces of an intact rotator cuff.

Glenoid erosion due to rotator cuff arthropathy represents a challenge during reverse shoulder arthroplasty. Incorrect positioning of the glenoid baseplate owing to deficient superior bone can result in residual superior tilt of the components. Superior tilt of the baseplate has been associated with an increased risk of aseptic loosening and instability.[9,10] Surgical techniques to address superior glenoid erosion in reverse shoulder arthroplasty include asymmetrical reaming, bone grafting, or the use of superiorly augmented baseplates.[8]

The current literature suggests that type E2 glenoid bone erosions are oriented purely superiorly as seen on standard anteroposterior radiographs or coronal computed tomography (CT) scans.[15] Roche et al[20] studied baseplate fixation for reverse shoulder arthroplasty in superiorly eroded type E2 glenoids using composite scapulae (Pacific Research Laboratories, Vashon, WA, USA), in which they created a purely superior glenoid defect. Our observational experience, viewing 3-dimensional (3D) CT scans and intraoperative assessments of type E2 glenoids, has raised the question of whether type E2 glenoid erosions follow a predictable pattern different from purely superior. An understanding of the orientation of bone loss in a typical type E2 glenoid has implications on baseplate fixation and the rotational orientation of an augmentation.

As such, the purposes of this study were 2-fold. The first purpose was to quantify glenoid erosion and orientation from CT scans of patients with type E2 glenoids. We hypothesized that type E2 erosion would not occur purely superiorly but would be oriented in a predictable posterosuperior direction. In addition, we hypothesized that the degree of fatty infiltration within the rotator cuff would influence the orientation of type E2 erosion. The second purpose of this study was to examine 4 commercially available reverse baseplate designs used for the management of type E2 erosions regarding the amount of bone volume removal necessary for proper seating: standard, half wedge, full wedge, and patient-matched (or BIO-RSA [Bony Increased Offset–Reverse Shoulder Arthroplasty]; Wright Medical Group, Memphis, TN, USA).

Materials and methods

Patients

Clinical CT scans (120-140 kV [peak], 512 × 512 resolution) were obtained from 51 patients with rotator cuff arthropathy and type E2 glenoid erosion. We excluded 11 patients because of low-quality scans or scans on which segmentation was not possible, leaving a total study cohort of 40 patients (28 women and 12 men) with a mean age of 74 years (range, 56-88 years). A type E2 glenoid was classified according to the Favard classification as any glenoid with erosion limited to the superior aspect and not extending as far as the inferior glenoid rim.[15,21] All CT scans were verified for the pathology in question by 2 board-certified and experienced surgeons (G.S.A. and G.W.).

Model creation

Each CT scan was uploaded as a DICOM (Digital Imaging and Communications in Medicine) file to an imaging software program (Mimics, version 16.0; Materialise, Leuven, Belgium). Through standard segmentation techniques validated by Bryce et al,[3] the humerus and clavicle were manually separated from the scapula to better visualize the glenoid. All segmentation in this study was performed by the same investigator (S.A.), trained in the use of the medical imaging software program. Subsequent to segmentation, 3D reconstructions of each patient's scapula were created as stereolithography files to allow study of glenoid erosion (Fig. 1).

Scapular anatomic reference planes were created by a modification of the method described by Frankle et al[6] to allow for consistent referencing between scapular models. A scapular plane was created using 3 anatomically identifiable points on the scapula: the center of the glenoid, the trigonum spinae, and the inferior angle. Perpendicular to this scapular plane and through the center of the glenoid, the sagittal plane was created to allow computational measurements.[6]

The anatomic landmarks of the supraglenoid and infraglenoid tubercles guided the creation of the superoinferior (SI) axis of the glenoid coordinate system (Fig. 2), against which the orientation of glenoid erosion was measured in later steps. This method has been validated previously.[14] The perpendicular bisector of this SI axis resulted in the anteroposterior axis of the glenoid, yielding the

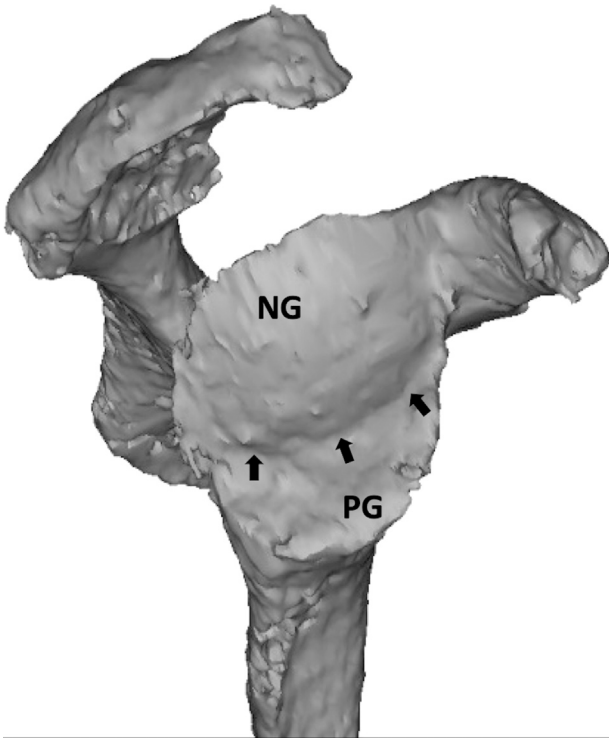

Figure 1 Three-dimensional sagittal view of a right-sided type E2 glenoid with posterosuperiorly oriented erosion and a curved line of erosion (⬅) separating the neoglenoid *(NG)* from the paleoglenoid *(PG)*.

center of the glenoid and simultaneously dividing the glenoid into 4 quadrants: anterosuperior, posterosuperior, anteroinferior, and posteroinferior.

Measurement of erosion orientation angle

The ridge of bone separating the paleoglenoid (original glenoid articular surface) from the eroded neoglenoid (newly eroded facet of the glenoid) was termed the ''line of erosion'' (Fig. 1). All forty 3D scapular models demonstrated a clearly defined curved line of erosion. This line of erosion was marked manually by 1 observer placing ten 3D point coordinates along its course (Fig. 2); the accuracy of the Mimics software program used in this study for anatomic measurements of the scapula has previously been validated by Bryce et al.[3] This step allowed for the creation of a circle of best fit. The 2 outermost points on the line of erosion, when connected, yielded the chord (c) of the circle. The radius (r) of the circle was placed orthogonally against the chord and, when extended, resulted in the orientation vector (v) of erosion. Ultimately, the angle (α) between this vector and the previously established SI axis resolved the erosion orientation angle. Thus, the vector of erosion indicated the overall erosion orientation and was described by its angle (α) from the SI axis.

To assess the extent of curvature of the line of erosion, the radius of the circle of best fit was calculated. A larger circle of best fit (with a corresponding larger radius) results from a set of coordinate points placed along a less curved (flatter) line of erosion. In contrast, a smaller circle of best fit (with a corresponding smaller radius) results from a more circular line of erosion. The computation of the aforementioned steps was facilitated by custom code developed in MATLAB (The MathWorks, Natick, MA, USA). The 3D point coordinates, the glenoid coordinate system, and the scapular and sagittal planes were extracted by the built-in MedCAD Mimics module (Materialise).

Surface area of erosion

To quantify the magnitude of glenoid erosion, the reconstructed 3D scapulae, in addition to the 10 point coordinates along the line of erosion, were exported into the 3-matic program (version 8.0; Materialise).[14] The articular surfaces of the neoglenoid and paleoglenoid were marked by the built-in surface highlighting tools. This allowed for automated calculation of the surface area of the selected regions on the glenoid articular surface. The surface area of the neoglenoid facet was computed as a percentage of the entire glenoid area (neoglenoid plus paleoglenoid). To allow for further comparison and statistical analysis, the severity of neoglenoid erosion was arbitrarily categorized into 3 subgroups, consisting of mild (0% to 33%), moderate (34% to 66%), and severe (>66%) erosion areas, as previously done in a similar quantification study.[4]

Rotator cuff fatty infiltration

The severity of fatty infiltration of the rotator cuff muscles (supraspinatus, infraspinatus, subscapularis, and teres minor) was classified according to the Goutallier classification[22] as follows: grade 0, no fat; grade 1, fatty streaks; grade 2, more muscle than fat; grade 3, equal muscle and fat; or grade 4, more fat than muscle. Fatty infiltration was visible by areas of decreased radiodensity using noncontrast CT scans in the sagittal-oblique view (''Y-view'') and was assessed by the senior author (G.S.A.), as previously described and validated.[7,18,23]

Type E2 reconstruction with augmented implants

The CT scans of a subgroup of 30 patients with type E2 erosion were exported in DICOM (Digital Imaging and Communications in Medicine) file format to allow for further processing in a preoperative planning software program (Glenosys; Imascap, Brest, France). This software automatically creates accurate and reproducible 3D reconstructions of the patient's scapula,[17,24] allowing for simulated implantation of various glenoid augmentation designs (Fig. 3).

The preoperative planning program allows the implantation of various reverse baseplate designs within specified parameters. All baseplates tested were circular and either 25 or 29 mm in diameter. The selection of the diameter of the baseplate and the glenosphere size (36, 39, or 42 mm) was made by an experienced shoulder surgeon (G.S.A.). Once the baseplate diameter and glenosphere size were selected for an individual patient, the same constructs were used for all scenarios with only the backside geometry of the implant varying. Four different backside baseplate designs were tested: standard, half wedge, full wedge, and patient-matched (Fig. 3). The standard baseplate was circular and flat backed. The half-wedge baseplate was circular and contained a half wedge that was slanted at 35°. The full-wedge baseplate was

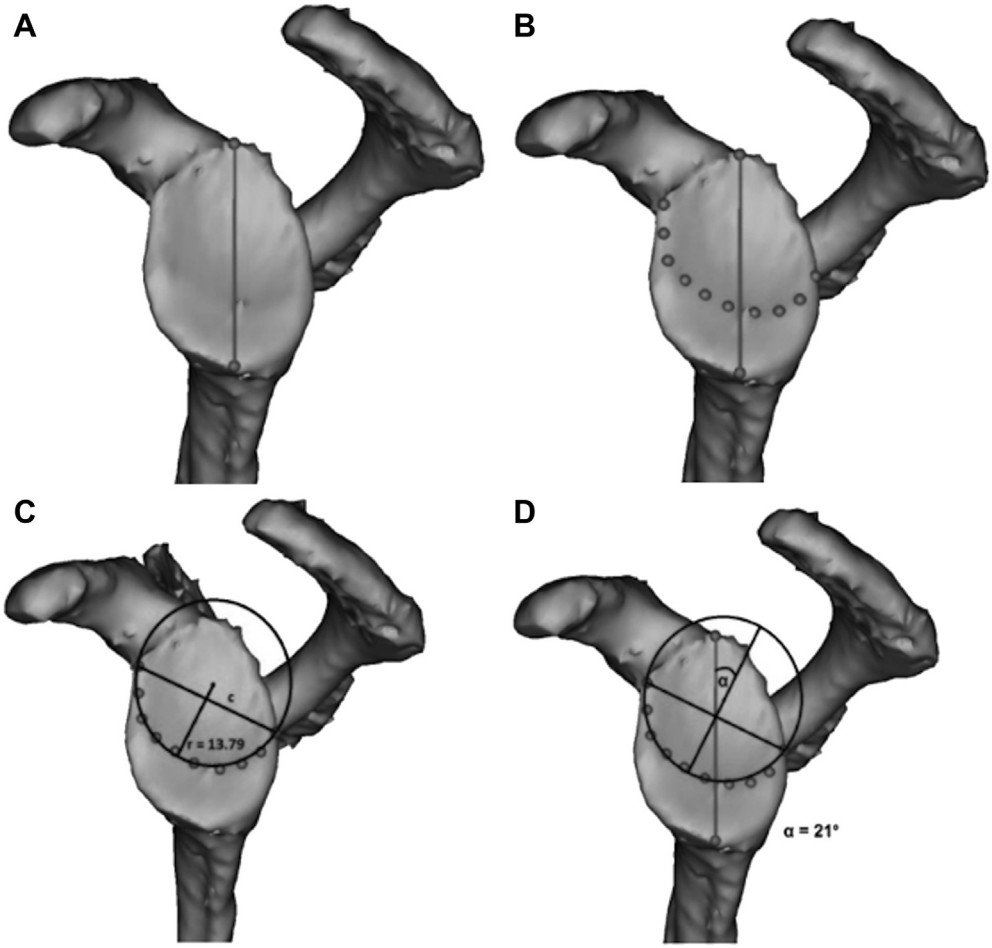

Figure 2 Determination of Favard type E2 erosion orientation. (**A**) The superoinferior axis of the glenoid is determined by the supraglenoid and infraglenoid tubercles as drawn. (**B**) Ten points are placed along the curved line of erosion separating the neoglenoid from the paleoglenoid. (**C**) The points are used to calculate the circle of best fit. Extending the radius *(r)* of the circle of best fit in a direction orthogonal to the chord *(c)* reveals the erosion vector. (**D**) The angle generated between the superoinferior axis and the erosion vector results in the erosion orientation angle *(α)*.

circular and contained a full wedge that was slanted at 15°. The patient-matched baseplate was circular with the backside geometry of the baseplate matching the patient's anatomy. The patient-matched baseplate design could also be used to represent a BIO-RSA design, as the patient-matched metal portion can also represent a patient-matched bone graft.[2]

All baseplates were implanted within predetermined parameters by the senior author (G.S.A.): 0° to 10° of retroversion, 0° of superior tilt, and greater than 80% backside seating on host glenoid bone. Each case (n = 30) was assessed without an implant and with all 4 baseplate implantations, for a total of 150 models. For each model, the volume of glenoid bone removal required for greater than 80% seating was determined by recording the volume of the scapular model (''scapula bone mask'') and the planned glenoid implant (''implant mask'') as a volumetric 3D binary image. Only the volume of bone removed in seating of the backside of the implant was determined, excluding the volume of the central post. Retrieving the common voxels between the scapula bone mask and the implant mask through voxel-by-voxel comparison yielded the final bone removal to be measured. Additional software outcome parameters, such as lateralization and bony impingement–free range of motion (adduction, abduction, flexion, extension, internal rotation, and external rotation), are automatically provided by the software and were recorded and compared between baseplate models. This bony impingement–free range of motion is merely a software-measured outcome and may not correlate with actual clinical range of motion, as true scapulothoracic movement or patient strength and muscle control generating such movements are not accounted for.

Statistical analysis

Demographic data and quantitative measures pertaining to erosion orientation in terms of angle and radii of curvature, surface area of erosion, and severity were reported as means and standard deviations for all 40 cases. Differences were evaluated using unpaired 2-sided *t* tests ($P < .05$). Linear regression analyses were performed for the following parameters: erosion orientation angle, severity of erosion, curvature of line of erosion, age, and sex. Range-of-motion comparisons between baseplate types were performed using a 1-way analysis of variance.

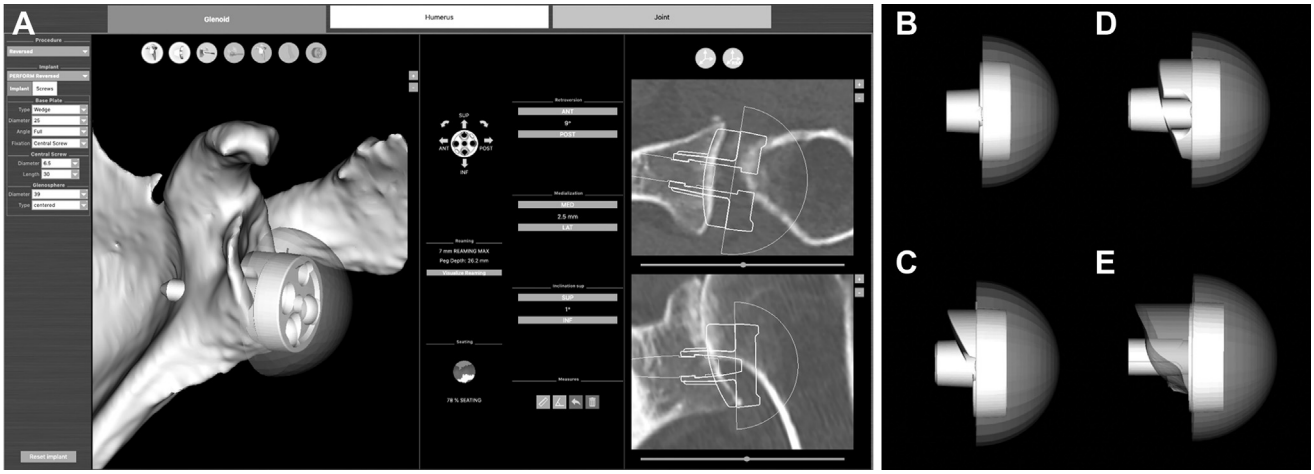

Figure 3 Screenshot view of surgical planning software (**A**) used to implant a standard baseplate (**B**), a half-wedge augmentation (**C**), a full-wedge augmentation (**D**), and a patient-matched glenoid baseplate (**E**). The patient-matched baseplate was used to represent a patient-specific 3-dimensionally printed implant or Bony Increased Offset–Reverse Shoulder Arthroplasty design. *ANT*, anterior; *POST*, posterior; *SUP*, superior; *INF*, inferior; *MED*, medial; *LAT*, lateral.

Results

The 40 type E2 glenoids were from 28 female (70%) and 12 male (30%) patients; the mean age was 74 years (range, 56-88 years). The difference in age between sexes was not statistically significant ($P = .68$). Of the shoulders, 27 (67.5%) were right shoulders and 13 (32.5%) were left shoulders.

Erosion orientation

The mean erosion orientation angle (α) between the vector of type E2 bony erosion and the SI axis of the glenoid was 47° ± 17° (range, 14°-74°) located in the posterosuperior quadrant of the glenoid, resulting in the average erosion being directed at 10:30 on a right-shoulder clock face (Fig. 4). The erosion orientation angle of type E2 bony erosion was not significantly different ($P = .38$) between women (48° ± 18°) and men (44° ± 14°). When we analyzed the orientation of the line of erosion by subgroup (mild, moderate, or severe), a steady decrease in the erosion orientation angle occurred as the severity of erosion increased. In the 1 example of mild erosion in our cohort, the angle of the erosion vector was 70°. The average erosion orientation angle (α) in the moderate group was 51° ± 15° and was not significantly different ($P = .37$) from that in the severe group, at 44° ± 17°.

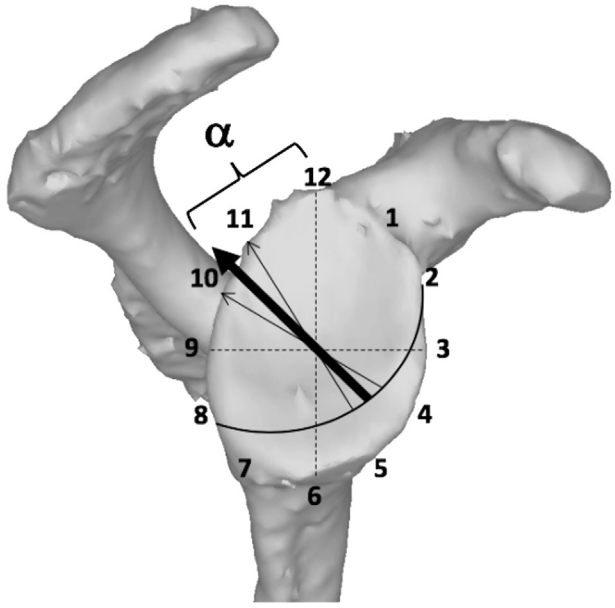

Figure 4 The mean type E2 bony erosion orientation angle *(α)* (± standard deviation) is located in the posterosuperior quadrant, measuring 47° ± 17° from the superoinferior axis (12- to 6-o'clock position) of the glenoid. This results in the average erosion being directed at 10:30 on a right-shoulder clock face. The ···· indicate the glenoid coordinate system (superoinferior and anteroposterior axes); –, line of erosion between the paleoglenoid and neoglenoid; ←, mean erosion orientation vector; and –, standard deviation of the erosion vector.

Surface area and line of erosion

In the entire group, the mean surface area of the neoglenoid was 636 ± 247 mm^2 (range, 233-1333 mm^2) and that of the paleoglenoid was 311 ± 165 mm^2 (range, 123-820 mm^2), revealing that, on average, the neoglenoids in the cohort consumed 67% of the total glenoid surface (average, 946 ± 209 mm^2). The neoglenoid erosion severity was mild in 1 case (3%), moderate in 14 (35%), and severe in 25 (63%). The corresponding surface area measurements by sex are presented in Table I. Women and men differed significantly regarding erosion severity ($P < .001$). The eroded neoglenoids occupied 61% ± 17% of the total glenoid area in

women and 78% ± 11% of that in men, corresponding to moderate and severe erosion patterns, respectively. No correlation was found between severity of erosion and age, erosion orientation angle, or radius of erosion curvature. The average radius of the circle of best fit for the curved line of erosion of the type E2 glenoids was 22 ± 6 mm (range, 13-36 mm).

Rotator cuff fatty infiltration

The distribution of fatty infiltration grades within each rotator cuff muscle is shown in Table II. The degree of fatty infiltration was severe (grade 4) in the supraspinatus muscle in 35 cases (88%) and in the infraspinatus muscle in 31 cases (78%). No subjects showed fatty infiltration of the supraspinatus or infraspinatus lower than grade 2. Within the subscapularis muscle, the majority of subjects (n = 18, 45%) showed grade 1 fatty infiltration, whereas 4 (10%) had grade 4 fatty infiltration. Grade 3 fatty infiltration of the subscapularis muscle was implicated in a mean erosion orientation angle of 58°, whereas grade 4 fatty infiltration of the subscapularis was associated with a significantly lower ($P < .001$) erosion orientation angle, at a mean of 24° (Fig. 5).

Augmented baseplate reconstruction

Significant differences ($P \leq .02$) were found between all 4 baseplate designs for the volume of bone removal required for greater than 80% seating on the type E2 glenoid (Fig. 6). The average volume of glenoid bone removed was significantly lower ($P \leq .01$) for the patient-matched (or BIO-RSA) design (mean, 200 ± 297 mm^3; range, 0-995 mm^3) and highest for the standard (non-augmented) design (mean, 4009 ± 1210 mm^3; range, 1954-6915 mm^3). The full-wedge design (1228 ± 753 mm^3; range, 354-3742 mm^3) removed significantly ($P = .02$) less bone volume than the half-wedge design (1763 ± 969 mm^3; range, 597-4290 mm^3). There were no significant differences in bone volume removal by sex in any of the 4 baseplate scenarios ($P \geq .38$).

The average implant data in terms of glenosphere and baseplate diameter, preoperative and postoperative glenoid version, global lateralization, and range-of-motion measurements for each baseplate design are listed in Table III for comparison. Significant differences in adduction occurred for all baseplate designs ($P < .001$), except between the patient-matched and full-wedge designs ($P = .575$). Equivalently, all baseplate designs differed significantly in external rotation ($P < .001$), except the patient-matched vs. full-wedge designs ($P = .803$). Significant improvements in extension were found between the patient-matched and standard designs, patient-matched and half-wedge designs, and full-wedge and standard designs ($P < .05$ for all). Similarly, significant improvements in flexion were noted between the patient-matched and standard designs ($P < .001$), full-wedge and standard designs ($P < .001$), and half-wedge and standard designs ($P < .001$). No significant differences in abduction ($P = .861$) or internal rotation ($P = .224$) were found between baseplate designs.

Table I Demographic and anatomic features of male and female patients with type E2 glenoid erosion

Measurement	Male patients (n = 12)	Female patients (n = 28)	*P* value
Age, yr	73 ± 9 (56-85)	74 ± 7 (62-88)	.68
Erosion orientation angle, °	44 ± 14 (24-64)	48 ± 18 (14-74)	.38
Radius of curvature, mm	20 ± 5 (15-31)	22 ± 6 (13-36)	.41
Area of erosion, %	78 ± 11 (severe)	61 ± 17 (moderate)	<.001*

Data are presented as mean ± standard deviation (range).
* Statistically significant.

Table II Goutallier grades of fatty infiltration of individual rotator cuff muscles in series

	Grade 0	Grade 1	Grade 2	Grade 3	Grade 4
Supraspinatus	—	—	1	4	35
Infraspinatus	—	—	5	4	31
Subscapularis	1	18	10	7	4
Teres minor	1	13	10	5	4

Data are presented as total number of cases.

Discussion

The results of this study indicate that the Favard type E2 erosion seen in cuff tear arthropathy does not occur purely superiorly on the glenoid but rather is oriented toward 10:30 on the clock face of a right shoulder, which corresponds to the posterosuperior glenoid quadrant. This finding supports our hypothesis that the neoglenoid in type E2 eroded glenoids is not purely directed toward the superior pole of the glenoid. We measured an average erosion orientation angle of 47° ± 17° from the SI axis, with all type E2 erosions in this study being contained within the posterosuperior glenoid quadrant. As such, surgeons considering bone grafting or the use of glenoid augmentations in type E2 cases should consider dialing the baseplate augmentation, or the bone graft, posterosuperiorly to minimize the bone preparation required for implant seating, as none of the subjects in our study exhibited a purely superior (12-o'clock) erosion orientation.

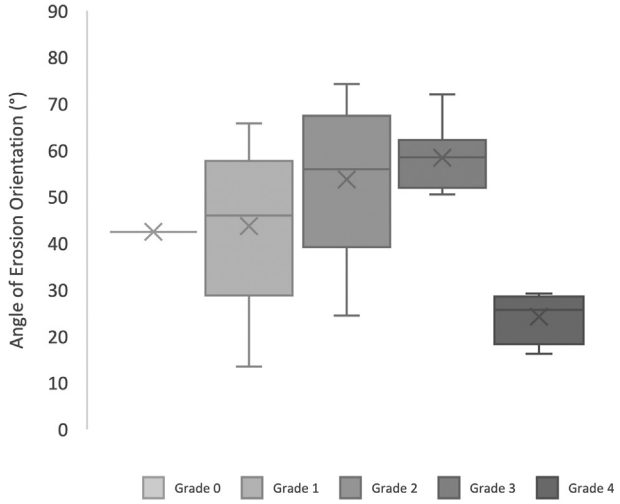

Figure 5 Subscapularis fatty infiltration grade vs. erosion orientation angle (in degrees) within cohort of type E2 eroded glenoids. A statistically significant decrease ($P < .001$) in the erosion orientation angle was found between patients with grade 4 fatty infiltration of the subscapularis and patients with lower grades. In the box plots, X indicates the mean; the horizontal line within the box marks the median. The lowest and highest boundary of the box represent the 25th and 75th percentile, respectively. The whiskers above and below the box are the 10th and 90th percentiles.

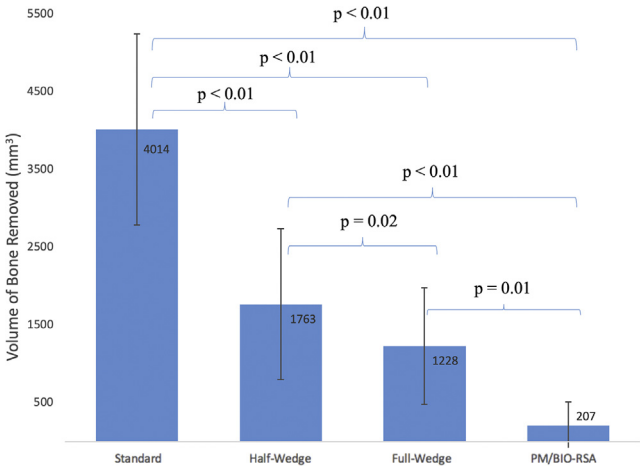

Figure 6 Average glenoid bone volume removed, with standard deviations represented as error bars, for a minimum of 80% backside seating of the 4 reverse baseplate designs: standard, half wedge, full wedge, and patient-matched *(PM)* or Bony Increased Offset–Reverse Shoulder Arthroplasty *(BIO-RSA)*. Differences in average bone volume removed between each augmented design reached statistical significance ($P < .05$).

When the ridge of bone between the paleoglenoid and neoglenoid—an interface we have termed the line of erosion—was examined, every patient in our cohort exhibited a curved line. Having a curved line of erosion seems logical, as the neoglenoid is formed by erosion caused by the hemispherical humeral head. As such, it would seem that rotation of the humeral head in the neoglenoid would lead to a concave erosion and a curved line of erosion. This information on the pathoanatomy of type E2 erosion may be important when considering future designs of augmented reverse baseplates or when using patient-matched technology.

In our type E2 cohort, the neoglenoid encompassed a larger-than-anticipated area on the glenoid, accounting for an average of 67% of the total glenoid surface. Given that reverse baseplate positioning is usually recommended to occur in the inferior two-thirds of the glenoid, poster-osuperior erosion of 67% of the total glenoid surface inevitably impacts baseplate positioning and may influence fixation. Martin et al[16] assessed the initial fixation stability in RSA baseplates by varying the extent of superior glenoid bone loss in foam bone models and found significantly reduced fixation when more than 50% of bone loss was present under the baseplate. In our series, with the mean surface area involvement of the glenoid being 67%, the use of a standard baseplate without high side reaming would always result in compromised initial fixation.

The reverse baseplate options tested in this study included a standard flat-backed circular baseplate, a half-wedge augmentation, a full-wedge augmentation, and a patient-matched augmentation (bone graft or metal). Our results, not surprisingly, showed that the patient-matched or BIO-RSA model resulted in significantly less glenoid bone removal and substantially more computationally determined range of motion in adduction, extension, and external rotation. In cases in which bone grafting may not be possible, such as revision surgery, severe cystic disease of the humeral head, or poor bone quality as in patients with rheumatoid disease, the use of an augmentation may be a preferable option.

The orientation of erosion becomes more relevant when considering commercially available augmentations such as half- and full-wedge components. In our study, between the 2 basic shapes of augmented components, we found the full-wedge design to be the more bone-preserving augmentation option in both men and women with moderate as well as severe erosion patterns. Some authors have reported on glenoid erosion augmentation options in posteriorly eroded type B2 glenoids and found the half-wedge component to be the most bone preserving.[1,11,13] Our results may differ from the type B2 literature owing to the curved nature of the type E2 line of erosion present in every case in our series. Commercially available wedged designs, even if oriented correctly toward the 10- or 11-o'clock position in type E2 glenoids, contain a straight-line decline in their step, whereas erosions in this study cohort were curved and, thus, may be a better fit for full-wedge augmentation. As intuitively expected and as previously concluded by other authors,[1,11,13] standard components were the least favorable option to account for asymmetrical glenoid bone loss when bone preservation was sought. The standard baseplate was also found to have the poorest computationally derived

range of motion, as measured by perimeter impingement by the planning software (Table III).

It is interesting to note that our results demonstrated that the volume of glenoid bone removed was highest among lower radii of erosion (more curved lines of erosion) in both the moderate and severe erosion subgroups. These results reveal that a straighter line of erosion produced less bone volume removal whereas a more curved line of erosion produced more bone volume removal during positioning of the baseplate scenarios used in our study. This finding may be related to different requirements for reaming when a curved line of erosion is present to adequately prepare the glenoid surface for proper seating of the baseplate. As such, a straighter erosion line requires less bone preparation to achieve sufficient osseous contact with a glenoid baseplate. In addition, when less glenoid bone removal is required for baseplate seating, more bone is preserved, resulting in a greater degree of glenoid lateralization, which may be beneficial for range of motion and the limitation of inferior notching.

The influence of rotator cuff fatty infiltration on the development of glenoid morphology has recently been studied. Donohue et al[5] retrospectively studied different patterns of pathologic glenoid bone loss in conjunction with rotator cuff muscle fatty infiltration and found increased fatty infiltration in association with type B3 glenoids and increased pathologic retroversion. Walker et al[25] demonstrated differences in fatty infiltration of the posterior rotator cuff between type A and type B glenoids. In our study, the degree of fatty infiltration was severe (grade 4) in the supraspinatus muscle in 35 cases (88%) and in the infraspinatus muscle in 31 cases (78%). This finding is consistent with the orientation of erosion toward the posterosuperior quadrant of the glenoid. These results, in agreement with the aforementioned studies, support the notion that there may be a causal relationship between fatty infiltration of the rotator cuff muscles and glenoid pathoanatomy, but the clinical relevance of this is still unknown. To investigate this further, we examined the degree of fatty infiltration of the subscapularis muscle and how it may affect erosion orientation. Although the majority of cases in this study demonstrated mild subscapularis muscle fatty infiltration, we found a marked difference in erosion orientation as the grade of fatty infiltration of the subscapularis muscle increased from grade 3 to grade 4. Grade 3 fatty infiltration of the subscapularis muscle was associated with a mean erosion orientation angle of 58° whereas grade 4 fatty infiltration of the subscapularis was associated with a mean erosion orientation angle of 24° from the SI axis on the glenoid ($P < .001$) (Fig. 5). We theorize that this change in erosion orientation toward a more superior direction may be due to chronic loss of subscapularis function, which results in an unrestrained superiorly directed force by the intact deltoid. With the subscapularis intact and the posterosuperior cuff absent, the force on the humeral head is directed posterosuperiorly, resulting in the posterosuperior erosions identified in this study. This theory, while interesting, is to be interpreted with a high degree of discretion given the small sample size provided in the subgroups of grade 3 and grade 4 subscapularis fatty infiltration.

Table III Implant parameters and post-implantation outcomes

	Data
Implant parameters	
All, n	30
Baseplate diameter, n	
25 mm	21
29 mm	9
Glenosphere diameter, n	
36 mm	11
39 mm	12
42 mm	7
Measurements	
Preoperative/postoperative glenoid version, mean, °	
Standard	12 retroversion/8 retroversion
Half wedge	12 retroversion/8 retroversion
Full wedge	12 retroversion/9 retroversion
Patient-matched	12 retroversion/9 retroversion
Final state: global lateralization, mm	
Standard	2
Half wedge	5
Full wedge	9
Patient-matched	10
Impingement-free range of motion: adduction/abduction/extension/flexion/IR/ER, °	
Standard	8*/78/32*/85*/66/22*
Half wedge	16*/81/52*/114*/77/41*
Full wedge	24*/84/80*/125*/79/53*
Patient-matched	25*/85/88*/125*/79/56*

IR, internal rotation; *ER*, external rotation.
* Indicates significant difference between baseplate designs ($P < .05$).

There are limitations to our study. One limitation is the number of patients in the study cohort, as we were only able to identify 40 patients with type E2 erosions and high-quality complete CT scans with full scapulae. In addition, the severity of glenoid erosion was measured by the area of erosion divided by the total glenoid area. This process does not account for the slope of erosion, represented by the inclination of the neoglenoid, which certainly is a contributing factor to the volume of bone loss actually present. Therefore, 2 glenoids with the same area of erosion may have very different volumes of bone loss present, and

this may not be taken into account by our definition of the severity of erosion. Although determining the depth of erosion (the inclination of the neoglenoid) may be interesting, it is not the focus of this study, in which we focused on the orientation of erosion in a type E2 glenoid for the purpose of determining the rotational orientation of a baseplate augmentation. In addition, this study focused on 1 set of commercially available augmented designs, and different baseplate morphologies exist, which may alter the results of our study. Moreover, our arbitrary division of the surface area of erosion into thirds represents a challenge for statistical analysis. Several of our values were close to the cutoff values; although we had only 1 mild case ($\leq$33% of area eroded), 3 further cases came very close to the cutoff value for mild (34% or 35% of area eroded). Finally, it is prudent to mention that it may seem as though this study contains a bias toward more moderate and severe erosion patterns, given that our study cohort contains only 1 mild case. An explanation for this, however, may be that superior migration of the humeral head in chronic rotator cuff deficiency is ultimately anatomically limited by the acromion, making truly mild erosion patterns that are primarily located in the superior one-third of the glenoid surface practically uncommon or nonexistent. Thus, it seems as though moderate to severe erosion patterns are more characteristic of the severity of wear seen in rotator cuff arthropathy owing to mere anatomic constraints of the superiorly migrated humeral head size on the glenoid surface.

Conclusion

This study demonstrated that the orientation of Favard type E2 glenoid erosion was not exclusively superior but rather was directed toward 10:30 on a right-shoulder clock face in the posterosuperior quadrant of the glenoid. In addition, the magnitude of fatty infiltration of the subscapularis muscle was associated with the orientation of glenoid bone loss. On comparison of reverse baseplate designs to manage type E2 erosions, the patient-matched or BIO-RSA design resulted in substantially less glenoid bone removal for implantation and significantly greater computationally assessed impingement-free range of motion. Finally, when full-wedge and half-wedge augmented implants were compared, the former resulted in significantly less bone removal.

Disclaimer

No company had any input into the study design, protocol, testing, data analysis, or manuscript preparation.

George S. Athwal is a consultant for Wright Medical-Tornier.

Gilles Walch is a consultant for Wright Medical-Tornier.

The other authors, their immediate families, and any research foundations with which they are affiliated have not received any financial payments or other benefits from any commercial entity related to the subject of this article.

References

1. Allred JJ, Flores-Hernandez C, Hoenecke HR, D'Lima DD. Posterior augmented glenoid implants require less bone removal and generate lower stresses: a finite element analysis. J Shoulder Elbow Surg 2016; 25:823-30. https://doi.org/10.1016/j.jse.2015.10.003
2. Boileau P, Moineau G, Roussanne Y, O'Shea K. Bony increased-offset reversed shoulder arthroplasty minimizing scapular impingement while maximizing glenoid fixation. Clin Orthop Relat Res 2011:2558-67. https://doi.org/10.1007/s11999-011-1775-4
3. Bryce CD, Pennypacker JL, Kulkarni N, Paul EM, Hollenbeak CS, Mosher TJ, et al. Validation of three-dimensional models of in situ scapulae. J Shoulder Elbow Surg 2008;17:825-32. https://doi.org/10.1016/j.jse.2008.01.141
4. Churchill RS, Spencer EE, Fehringer EV. Quantification of B2 glenoid morphology in total shoulder arthroplasty. J Shoulder Elbow Surg 2015;24:1212-7. https://doi.org/10.1016/j.jse.2015.01.007
5. Donohue KW, Ricchetti ET, Ho JC, Iannotti JP. The association between rotator cuff muscle fatty infiltration and glenoid morphology in glenohumeral osteoarthritis. J Bone Joint Surg Am 2018;100:381-7. https://doi.org/10.2106/JBJS.17.00232
6. Frankle MA, Teramoto A, Luo ZP, Levy JC, Pupello D. Glenoid morphology in reverse shoulder arthroplasty: classification and surgical implications. J Shoulder Elbow Surg 2009;18:874-85. https://doi.org/10.1016/j.jse.2009.02.013
7. Fuchs B, Weishaupt D, Zanetti M, Hodler J, Gerber C. Fatty degeneration of the muscles of the rotator cuff: assessment by computed tomography versus magnetic resonance imaging. J Shoulder Elbow Surg 1999;8:599-605.
8. Gilot GJ. Addressing glenoid erosion in reverse total shoulder arthroplasty. Bull NYU Hosp Jt Dis 2013;71(Suppl 2):51-3. https://doi.org/10.2307/1928969
9. Gutiérrez S, Greiwe RM, Frankle MA, Siegal S, Lee WE. Biomechanical comparison of component position and hardware failure in the reverse shoulder prosthesis. J Shoulder Elbow Surg 2007; 16(Suppl):S9-12. https://doi.org/10.1016/j.jse.2005.11.008
10. Gutiérrez S, Walker M, Willis M, Pupello DR, Frankle MA. Effects of tilt and glenosphere eccentricity on baseplate/bone interface forces in a computational model, validated by a mechanical model, of reverse shoulder arthroplasty. J Shoulder Elbow Surg 2011;20:732-9. https://doi.org/10.1016/j.jse.2010.10.035
11. Kersten AD, Flores-Hernandez C, Hoenecke HR, D'Lima DD. Posterior augmented glenoid designs preserve more bone in biconcave glenoids. J Shoulder Elbow Surg 2015;24:1135-41. https://doi.org/10.1016/j.jse.2014.12.007
12. Klein SM, Dunning P, Mulieri P, Pupello D, Downes K, Frankle MA. Effects of acquired glenoid bone defects on surgical technique and clinical outcomes in reverse shoulder arthroplasty. J Bone Joint Surg Am 2010;92:1144-54. https://doi.org/10.2106/JBJS.I.00778
13. Knowles NK, Ferreira LM, Athwal GS. Augmented glenoid component designs for type B2 erosions: a computational comparison by volume of bone removal and quality of remaining bone. J Shoulder Elbow Surg 2015;24:1218-26. https://doi.org/10.1016/j.jse.2014.12.018

14. Knowles NK, Keener JD, Ferreira LM, Athwal GS. Quantification of the position, orientation, and surface area of bone loss in type B2 glenoids. J Shoulder Elbow Surg 2015;24:503-10. https://doi.org/10.1016/j.jse.2014.08.021
15. Lévigne C, Boileau P, Favard L, Garaud P, Molé D, Sirveaux F, et al. Scapular notching in reverse shoulder arthroplasty. J Shoulder Elbow Surg 2008;17:925-35. https://doi.org/10.1016/j.jse.2008.02.010
16. Martin EJ, Duquin TR, Ehrensberger MT. Reverse total shoulder glenoid baseplate stability with superior glenoid bone loss. J Shoulder Elbow Surg 2017;26:1748-55. https://doi.org/10.1016/j.jse.2017.04.020
17. Moineau G, Levigne C, Boileau P, Young A, Walch G. Three-dimensional measurement method of arthritic glenoid cavity morphology: feasibility and reproducibility. Orthop Traumatol Surg Res 2012;98(Suppl):S139-45. https://doi.org/10.1016/j.otsr.2012.06.007
18. Müller CT, Buck FM, Mamisch-Saupe N, Gerber C. Good correlation of Goutallier rating of supraspinatus fatty changes on axial and reformatted parasagittal computed tomographic images. J Comput Assist Tomogr 2014;38:340-3. https://doi.org/10.1097/RCT.0000000000000059
19. Neer CS II, Craig EV, Fukuda H. Cuff-tear arthropathy. J Bone Joint Surg Am 1983;65:1232-44.
20. Roche CP, Stroud NJ, Martin BL, Steiler CA, Flurin PH, Wright TW, et al. Achieving fixation in glenoids with superior wear using reverse shoulder arthroplasty. J Shoulder Elbow Surg 2013;22:1695-701. https://doi.org/10.1016/j.jse.2013.03.008
21. Sirveaux F, Favard L, Oudet D, Huquet D, Walch G, Molé D. Grammont inverted total shoulder arthroplasty in the treatment of glenohumeral osteoarthritis with massive rupture of the cuff. J Bone Joint Surg Br 2004;86:388-95. https://doi.org/10.1302/0301-620X.86B3.14024
22. Somerson JS, Hsu JE, Gorbaty JD, Gee AO. Classifications in brief: Goutallier classification of fatty infiltration of the rotator cuff musculature. Clin Orthop Relat Res 2016;474:1328-32. https://doi.org/10.1007/s11999-015-4630-1
23. Trudel G, Ryan SE, Rakhra K, Uhthoff HK. Extra- and intramuscular fat accumulation early after rabbit supraspinatus tendon division: depiction with CT. Radiology 2010;255:434-41. https://doi.org/10.1148/radiol.10091377
24. Walch G, Vezeridis PS, Boileau P, Deransart P, Chaoui J. Three-dimensional planning and use of patient-specific guides improve glenoid component position: an in vitro study. J Shoulder Elbow Surg 2015;24:302-9. https://doi.org/10.1016/j.jse.2014.05.029
25. Walker KE, Simcock XC, Jun BJ, Iannotti JP, Ricchetti ET. Progression of glenoid morphology in glenohumeral osteoarthritis. J Bone Jt Surg Am 2018. https://doi.org/10.2106/JBJS.17.00064